Experimental study of passive defect localization in plates using ambient noise

Lynda Chehami, Julien de Rosny, Claire Prada, Emmanuel Moulin, Jamal Assaad

IEEE TRANSACTIONS ON ULTRASONICS, FERROELECTRICS, AND FREQUENCY CONTROL,
vol. 62, no. 8, AUGUST 2015

Experimental Study of Passive Defect Localization in Plates Using Ambient Noise

Lynda Chehami, Julien de Rosny, Claire Prada, Emmanuel Moulin, and Jamal Assaad

***Abstract*—Passive listening methodology has been shown to be a practical and effective method for passive structural health monitoring. In this work, this approach is applied experimentally to monitor the occurrence of defects in thin aluminum plates. A correlation matrix is estimated from noise vibrations recorded on a transducer array. A defect is localized by applying a beamforming algorithm to the difference between the correlation matrices obtained with and without the defect. We successfully detect defects for different kinds of noise sources. Moreover, we show that this technique is robust to detect massive inclusions, holes, and cracks. With a vibrometer, we observe that the fidelity of the estimated transient responses strongly depends on the number of uncorrelated noise sources. Finally, we show that the defect is successfully localized even if the noise source distribution is not uniform, provided that it remains spatially stationary between the states with and without defect. A simple theoretical framework is proposed to interpret these results.**

I. Introduction

In everyday life, we naturally derive benefit from noise sources. Indeed, the eyes build an image from the noise radiation emitted by the sun, for instance. In underwater acoustics, vessels can be localized by beamforming the noise that they generate. However, in 2001, Weaver and Lobkis proposed a new way to exploit noise fields [1]. They have experimentally shown on an aluminum block that the cross-correlation of elastic noise between two receivers provides the transient response between the two receiver positions as if one of them acted as an elastic transient source. For very wideband noise sources, the transient response can be interpreted as the Green's function G. This result takes its roots in the fluctuation-dissipation theorem [2], [3]. This property is not limited to thermal noise sources, but applies to any noise source distribution that generates an equipartitioned wave-field [4].

In fact, in some situations it is desirable to avoid the need for active energy sources, so the major interest of this result is the estimation of the transient response without requiring any energy source. This property had been used implicitly before 2001. For instance, in seismology, Weller [5] proposed a patent in 1974, and Claerbout [6] extracted ground layer information from ambient seismic noise correlation in 1968. More recently, by cross-correlating the fluctuations of light emitted at the surface of the sun, Duvall *at al.* [7] deduced the internal structure of the sun. The main application of the Green's function extraction from the noise correlation function (NCF) is in seismology, where Artman [8] and Shapiro and Campillo [9] have demonstrated the universal interest. Passive Green's function estimation also offers promising applications in other domains ranging from ultrasound [10], [11] and underwater acoustics [12], [13] to medical imaging [14]. Only a few works are devoted to structural health monitoring. In this field, a pioneer work consisted of using the traffic excitation to recover resonant frequencies and modal damping of a bridge from noise cross-correlation [15]. Later, this approach has been applied to extract the Rayleigh–Lamb Green's transient responses on plates [16], [17]. The method is sufficiently sensitive to observe the elastic signature of a plate defect on the cross-correlation [16]. To localize a defect, an original method has been proposed [18] that is particularly efficient when the noise source distribution is not uniform. Recently, based on numerical simulation results, we have shown that we can apply a simple beamforming algorithm on the correlation matrix recorded by an array of transducers to efficiently localize a defect [19].

In this work, for the first time, we experimentally validate this approach for the detection of defects in aluminum plates between 10 and 40 kHz. Several artificial defects are successfully detected: metallic cylinders, holes, and cracks.

The paper is organized as follows. In Section II, we study the accuracy of the Green's function estimation with respect to the number of uncorrelated noise sources, using a laser vibrometer. In Section III, a pair of cylindrical magnets is used as a defect. The correlation matrix is measured with and without the defect. The beamforming is then processed on the differential correlation matrix, leading to a precise localization of the defect. Several kinds of noise sources are tested: controlled or natural sources. In Section IV, we show that the method is still robust for localizing more realistic defects such as holes, massive inclusions, or even cracks. Finally, in Section V, the effect of the distribution, the stationarity, and the number of noise sources on the ability to localize a defect is quantified.

L. Chehami, E. Moulin, and J. Assaad are with the Institut d'Electronique de Microélectronique et de Nanotechnologie (IEMN) UMR CNRS 8520, Université de Valenciennes et du Hainaut-Cambrésis, F-59313 Valenciennes Cedex 9, France (e-mail: chehamily@hotmail.fr).

J. de Rosny and C. Prada are with the Institut Langevin, École Supérieure de Physique et de Chimie Industrielles de la Ville de Paris (ESPCI), CNRS, UMR 7587, F-75231 Paris Cedex 5, France.

DOI http://dx.doi.org/10.1109/TUFFC.2014.006935

II. Green's Function Retrieval From a Finite Number of Sources on Plate

In thin plates, because of top and bottom stress-free boundary conditions, only three thickness modes can propagate: S_0, SH, and A_0 [20]. At very low frequency, the A_0 mode, also called flexural mode, dominates the normal displacement and is preferentially generated by surface excitation. In highly reverberating plates (low acoustic attenuation), the three modes (and in particular A_0, which we are mainly interested in here, for the reasons invoked previously) undergo multiple reflections at the boundaries.

We assume that there are N_s uncorrelated noise sources distributed over the plate, and that all of them have the same statistical properties. By definition, the cross-correlation of the normal components of flexural noise field recorded by two receivers at positions $\mathbf{r}_i$ and $\mathbf{r}_j$ is given by

$$C_{ij} = \sum_{k=1}^{N_s} G(\mathbf{r}_i, \mathbf{r}_k, -t) \otimes G(\mathbf{r}_j, \mathbf{r}_k, t) \otimes R_n(t), \qquad (1)$$

where $G(\mathbf{r}_i,\mathbf{r}_k,t)$ is the Green's function from point $\mathbf{r}_k$ to point $\mathbf{r}_i$, R_n is the auto-correlation of the noise generated by each source, and $\otimes$ denotes convolution.

By decomposing the field over the eigenmodes of the plate, we have shown that the correlation function can be expressed [19] as

$$C_{ij}(t) = [G(\mathbf{r}_i, \mathbf{r}_j, t) - G(\mathbf{r}_i, \mathbf{r}_j, -t)] \otimes f(t) + n_{ij}(t), \qquad (2)$$

where the time-dependent function $f(t)$ can be seen as an equivalent source term that can be expressed as

$$f(t) = \frac{N_s \tau_a}{2S\rho h} \int_{-\infty}^{t} R_n(\tau)\, d\tau,$$

where h is the plate thickness, ρ is the volume density, and S is the plate surface area. All kinds of loss (intrinsic dissipation, acoustic emission in air) are included in the damping term τ_a.

Eq. (2) means that the Green's function between the two measurement points is contained in the cross-correlation of passive recordings at the same points. However, the cross-correlation also includes an unwanted term $n_{ij}(t)$ that degrades the estimation of the Green's function. Its full expression involves cross-modal terms [19]. We have shown that the larger the number of noise sources, the smaller this unwanted term. It should be noted that if the noise sources are uniformly distributed over the plate surface (idealized case), then $n_{ij}(t)$ is zero.

We propose to experimentally validate and quantify this result, but because it is difficult to control numerous uncorrelated noise sources, we will estimate the cross-correlation function using the reciprocity theorem. Considering a time-dependent (deterministic) function q such as $q(\tau) \otimes q(-\tau) = R_n(\tau)$, (1) can be rewritten as

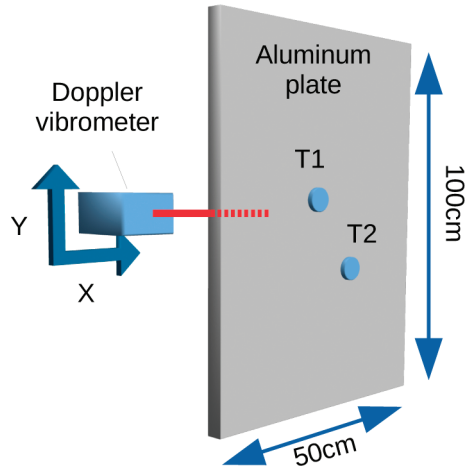

Fig. 1. Schematic view of the experiment: two thin transducers, T1 and T2, are glued on one side of a 3-mm-thick plate. On the other side, a Doppler vibrometer mounted on an X-Y displacement stage records the normal velocity.

$$C_{ij} = \sum_{k=1}^{N_s} [G(\mathbf{r}_k, \mathbf{r}_i, -t) \otimes q(-t)] \otimes [G(\mathbf{r}_k, \mathbf{r}_j, t) \otimes q(t)]. \qquad (3)$$

In other words, the correlation function C_{ij} can be equivalently estimated by using the receivers as emitters and recording the signal at chosen "source" locations.

The corresponding setup is shown in Fig. 1. The study is performed on a 3-mm-thick aluminum plate of 100 × 50 cm^2 size. Two transducers (T1 and T2) are glued on the plate at positions $\mathbf{r}_1$ and $\mathbf{r}_2$ and will be successively fed by a signal $q(t)$ generated by an arbitrary waveform generator. On the other side, the normal velocity is recorded by a Polytec laser vibrometer (OFV 505, Polytec GmbH, Waldbronn, Germany; velocity decoder with cut-off frequency of 250 kHz) mounted on a two-axis displacement stage and the sampling rate is fixed by the acquisition card (MOTU 828X, MOTU Inc., Cambridge, MA, USA) at 96 kHz. In this manner, 2-D scans of the transient responses induced successively by both transducers are recorded. The transient responses are recorded at 170 points inside a 90 × 45 cm rectangle (therefore covering almost the whole plate surface), with a spatial sampling interval of 5 cm. We collect 170 × 2 transient responses: $G(\mathbf{r}_i,\mathbf{r}_k,t) \otimes q(t)$, with $k = (1,\ldots,170)$ and $i = (1,2)$. By selecting random subsets inside the 170 responses, we can study the effect of the number of noise sources N_s on the quality of the transient response estimations. To increase the signal-to-noise ratio, we use a pulse-compression technique. Thus, the emitted signal $q(t)$ is a 62.5-μs-long chirp with a linear frequency modulation ranging from 100 Hz to 40 kHz, whose autocorrelation is a short-duration time function. Then the experimental correlation function C_{12} can be constructed according to (3). (Note that because we use only two transducers in this experiment, we set $i = 1$ and $j = 2$.)

For positive times, we can compare the correlation function C_{12} to the causal term $G(\mathbf{r}_1,\mathbf{r}_2,t) \otimes f(t)$ of (2)

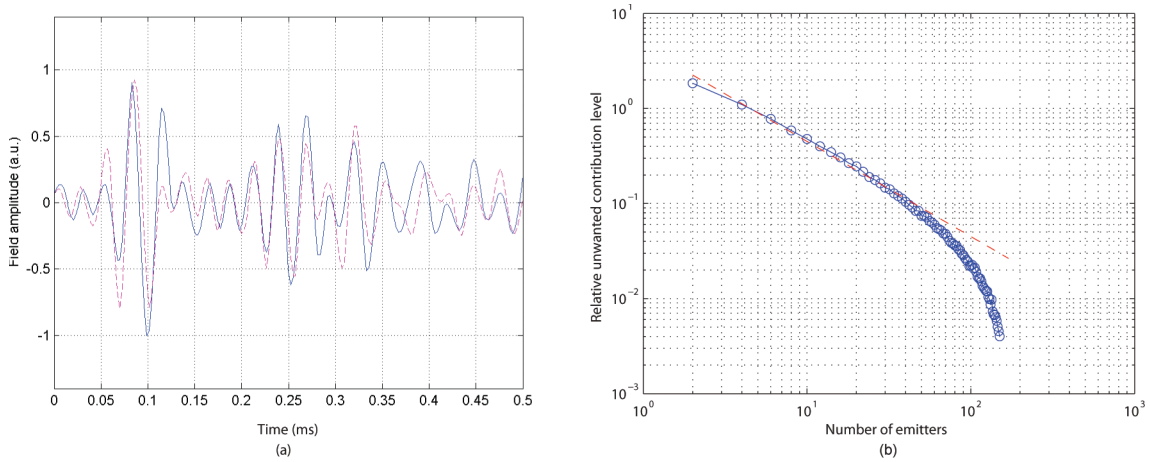

Fig. 2. (a) Cross-correlation C_{12} obtained with 170 virtual sources plotted for positive time (blue curve) and the active transient response (magenta dashed line). (b) Plot of the RNL defined in (4) (the relative unwanted contribution level) (blue line), fitted by a $1/N_s$ law (red dashed line) in logarithmic scale.

(denoted as the active transient response; see [19] for more details). This comparison is shown in Fig. 2(a), for $N_s = 170$ noise sources. The agreement is very good, showing an efficient passive reconstruction of the Green's function (at least in the considered frequency range) because of a significant reduction of the unwanted term n_{12}.

Now we will take this correlation for the 170 sources as a reference (denoted C_{12}^{∞}), in the objective of quantifying the degradation of the reconstruction when the number of sources N_s decreases. Therefore, we compute the following relative-to-noise level (RNL), for different values of N_s:

$$\mathrm{RNL}(N_s) = \frac{\int (C_{12}^{N_s} - C_{12}^{\infty})^2 \mathrm{d}t}{\int (C_{12}^{\infty})^2 \mathrm{d}t}, \qquad (4)$$

where $C_{12}^{N_s}$ is the experimental correlation obtained by summing over N_s virtual noise sources.

This RNL of the passive Green's function reconstruction is represented (logarithmic scale) in Fig. 2(b), as a function of N_s (in blue). It can be observed that the obtained curve is well fitted by a $1/\sqrt{N_s}$ law (red dashed line). This can be explained by the fact that for a small number of noise sources, the unwanted term n_{12} can be approximately described as a sum of N_s uncorrelated zero-mean random values. In consequence, its energy grows linearly with N_s. The energy of the term $G \otimes f$ [see (2)] increases naturally as N_s^2. These considerations explain why the RNL varies as $1/N_s$ on Fig. 2(b) when $N_s < 50$. For larger N_s values, the assumption of uncorrelated sources might become doubtful and the fact that the chosen reference C_{12}^{∞} is slightly different from the perfectly reconstructed GF (i.e., G_{12}) makes the experimental curve differ from the theoretical $1/N_s$ law.

Finally, it should be noted that the Heisenberg time T_H (or modal density) for the plate considered here is approximately 50 ms, which is slightly lower than the reverberation time T_R (approximate signal duration). In the opposite case ($T_R < T_H$), the modes would not be resolved whatever the recording time. However, this would not prevent accurate reconstruction of the Green's functions, provided that all of the transient response is recorded and there are enough noise sources, as will be observed in the experiments of the next section.

III. Application to Defect Localization

As shown numerically in a previous work [19], this principle of passive Green's function reconstruction can be used to localize a local change (defect) in a plate. In this section, we intend to confirm this possibility experimentally under various noise source conditions.

The experiment is performed on a 3-mm-thick aluminum plate of dimensions 1.5 m by 1 m (see Fig. 3). The corresponding T_H is of the order of 160 ms. However, because T_R is approximately 35 to 40 ms, the recording time will be set to 40 ms, which will be sufficient here, as will be observed. To minimize the coupling with the support, the plate is isolated from the table with polystyrene blocks. Eight transducers are glued on the plate surface. In this experiment, they are approximately equally distributed on a quasi-circular contour. This particular shape

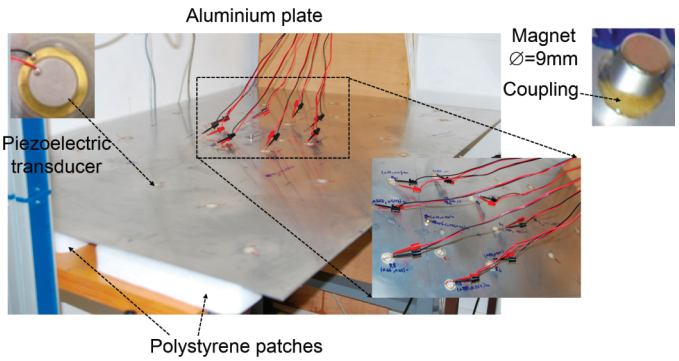

Fig. 3. Experimental setup: the eight piezoelectric transducers are used only in reception.

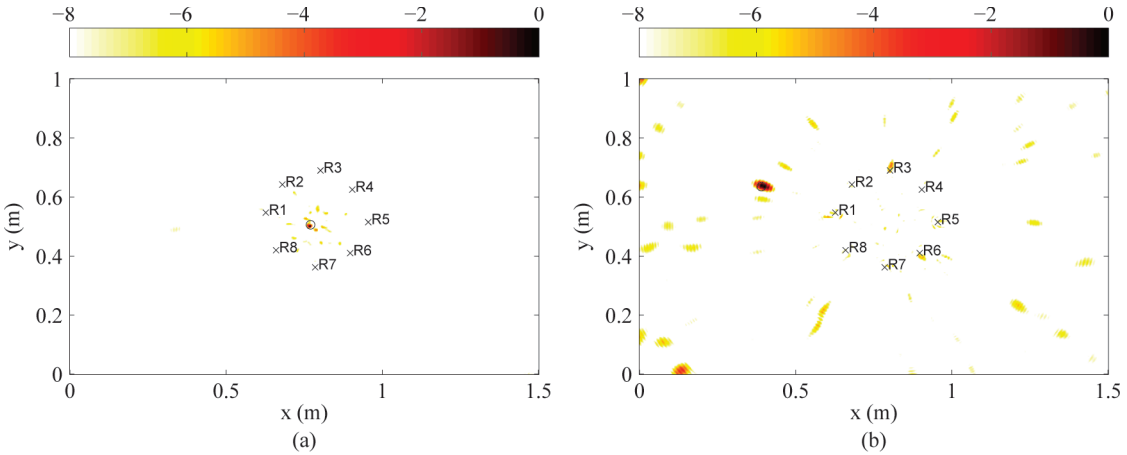

Fig. 4. Beamformed images obtained for two defect locations (circles) in decibels. The correlation matrix is built from the signals recorded on 8 transducers (crosses). The vibrations are successively generated by 20 transducers (not shown) that are arbitrarily distributed over the plate.

has been chosen to define interior and exterior domains in an unambiguous way, and to avoid any preferential direction. Note however that using a more arbitrary transducer array shape should not fundamentally change the localization results, provided the spatial step and the total aperture are of the same order. First we use defects that can be removed. The reversible defects consist of two cylindrical magnets facing each other on opposite sides of the plate (diameter 9 mm, height 10 mm) and coupled to the plate with honey. This constitutes a practical means of applying a local heterogeneity on the plate, and it can therefore be used to test several defect positions without actually damaging the plate.

Because the echo of the defect is very weak compared with the reverberated flexural waves, it is necessary to use a subtraction between the defect-free case and the case in which the defect is applied to the plate. To that end, a first acquisition of the responses between the N_R transducers (here $N_R = 8$) is achieved without the defect. Thus, a reference matrix $\mathbf{C}^{\text{ref}}(t)$ of 8 by 8 correlation terms is collected. Then the correlation matrix $\mathbf{C}^{\text{def}}(t)$ is measured with the defect added. The effect of the defect is contained in the differential matrix $\Delta\mathbf{C}(t)$, which is equal to $\mathbf{C}^{\text{def}}(t) - \mathbf{C}^{\text{ref}}(t)$.

Then, assuming $\Delta\mathbf{C}(t)$ is sufficiently close to the differential Green's functions matrix, a beamforming algorithm is applied to localize the defect. The principle of this algorithm has been described in detail in a previous work [19]. We summarize here only the main points. First, from the Fourier transform of $\Delta\mathbf{C}(t)$, a back-propagation function $\text{bpf}(\omega)$ is defined for each pixel (x, y) position as

$$\text{bpf}_{(x,y)}(\omega) = \sum_{n=1,m=1}^{N_R,N_R} \Delta C_{nm}(\omega) \exp[j[d_n(x,y) + d_m(x,y)]k(\omega)], \tag{5}$$

where $k(\omega)$ is the wavenumber corresponding to the flexural waves (A_0 Lamb mode) and $d_n(x,y)$ [respectively, $d_m(x, y)$] is the distance between the transducer number n (respectively, number m) and the position of coordinates (x,y) on the plate.

Then we perform the inverse Fourier transform of bpf and compute the image intensity at pixel (x,y) as

$$I(x,y) = \int_{-T_0/2}^{T_0/2} \left|\text{bpf}_{(x,y)}(t)\right|^2 \mathrm{d}t, \tag{6}$$

where T_0 is the inverse of the noise bandwidth. For more details about the algorithm, see [19].

In the following sections, we show localization results obtained with several kinds of noise sources: distributed point-sources, friction noise, and air-coupled acoustic noise.

A. Localization With a Set of Arbitrary Point-Like Sources

We first validate the approach with a set of arbitrarily-placed sources, as was done with the numerical simulations in a previous work [19]. To that end, twenty broadband piezoelectric transducers are arbitrarily placed over the plate surface (see Fig. 3). Instead of emitting noise, the 20 broadband sources emit successively identical signals $q(t)$ corresponding to one sinusoidal period at 20 kHz (which yields a frequency range approximately between 10 kHz and 30 kHz, where the A_0 Lamb mode is predominant). For each pulse emission, 8 transient responses are simultaneously recorded on the 8 receivers. The signals are digitized by a 24-bit, 96 kSample/s acquisition card for 40 ms. From these 20 × 8 responses, we can build an 8 × 8 element matrix for each source. Then, by summing these twenty matrices, we obtain a total correlation matrix $\mathbf{C}$ similar to the one that would have been obtained if the 20 noise sources emitted completely uncorrelated noise.

Using this procedure, the differential correlation matrix (difference between the plate with and without the defect) is obtained. The result of the beamforming algorithm of $\Delta\mathbf{C}$ is shown in Fig. 4. For more clarity, the intensity $I(x, y)$ is represented in decibel scale. Tests for two defect

positions are presented here. One defect is located inside the 8-receiver array and the other defect is outside. In both cases, the defect position is recovered. The resolution and the spurious lobe levels are smaller when the defect is inside the receiver array than outside. This is a classical result in array processing. Indeed, in the first case, the spurious lobe level is smaller because all the receivers contribute to the beamforming processing. Moreover, as the transducers completely surround the defect, the best resolution is achieved, i.e., it is given by half the central wavelength. In the second case, the spurious lobes are stronger and the resolution is degraded because the distance between the array and the defect reaches the same order of magnitude as the array aperture.

B. Localization With Ambient Noise Sources

In this section, we deal with more realistic vibration noise sources. Note that the precise knowledge of the noise source is not necessary in this passive experiment. The first noise source is generated by friction and the second noise source results from the coupling with an acoustic noise source. However, in practice, the noise sources may not be temporally stationary and may show strong frequency fluctuations. To mitigate these two effects, two operations are performed on the raw signals before the correlation process. First, the amplitude of the envelope of time-dependent noise is normalized to compensate the temporal fluctuations. Second, a frequency whitening is performed on the obtained signals between 0.5 and 30 kHz.

To estimate the differential correlation matrix, the 8 receivers record the ambient noise for $T = 60$ s. This duration, much larger than the reverberation and Heisenberg times, has been empirically adjusted to obtain sufficient signal-to-noise ratio in the noise correlation functions. The operation is performed one time without the defect and one time with the defect. Then the subtraction of the correlation matrices is performed.

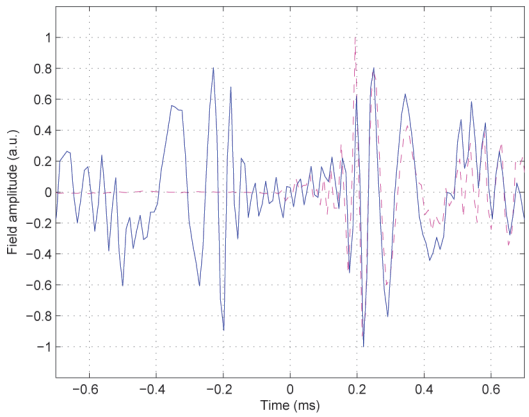

Fig. 5. Typical cross-correlation between transducers 1 and 8 obtained with frictional noise (blue line) compared with the primitive transient response directly measured between the same pair of transducers (magenta dashed line).

1) Frictional Noise: The frictional noise was produced on the plate by rubbing continuously and manually the whole plate surface with a soft scrubbing pad. A typical result of the cross-correlation between two channels is plotted in Fig. 5 for the frictional noise case. The transient response directly recorded when one of the two transducers acts as a source is plotted on the same figure (magenta dashed line).

The excellent agreement confirms the ability to passively estimate the transient response using this particular type of noise. This is confirmed by the successful localization results shown on Fig. 6 for two different defect positions.

2) Acoustic Noise: Next, a pseudo-random wideband noise was generated using a wireless loudspeaker. While emitting the noise, the loudspeaker was continuously moved all over the plate at a distance of about 10 to 20 cm from the surface. We observe on Fig. 7 that the defect detection is even more efficient than the one obtained with frictional noise.

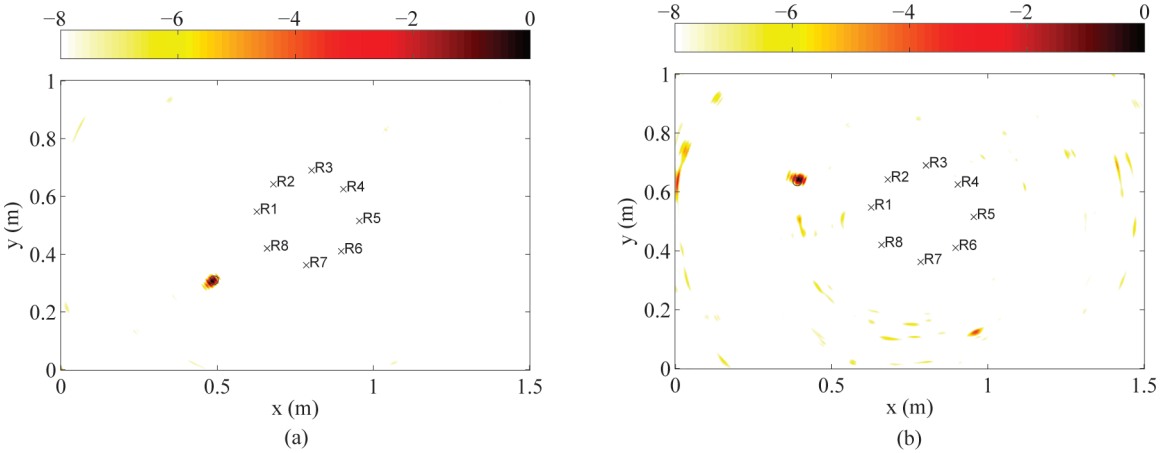

Fig. 6. Beamformed images obtained from frictional noise correlation for a defect located at positions (a) (0.49,0.31) m and (b) (0.39,0.635) m, in decibels.

DOI http://dx.doi.org/10.1109/TUFFC.2014.006935

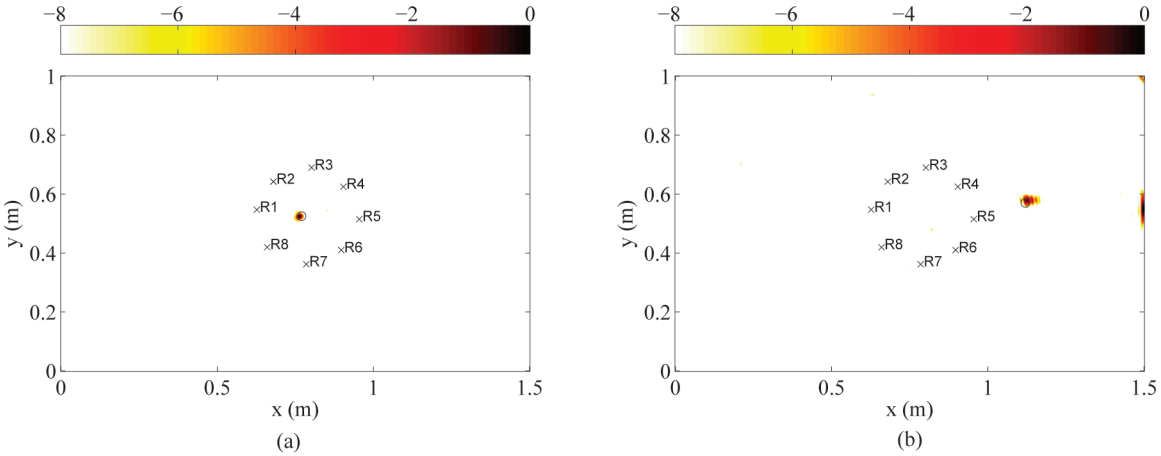

Fig. 7. Beamformed images obtained from acoustic noise correlation for a defect located at positions (a) (0.77,0.525) m and (b) (1.12,0.57) m, in decibels.

Note that a strong spurious lobe is observed on the right side of the plate in Fig. 7(b). This is a shadow effect. Indeed, because of energy conservation, when we subtract the two correlation matrices, the part of the signal that is reflected off the scatterer induces a decrease of the scattered echo from the boundary in the alignment of the array and the defect location.

IV. Localizing Holes, Inclusions, and Cracks

In this section, we intend to test the passive defect localization technique on more realistic defect types. Material fatigue often appears in the form of local change of physical properties. Therefore, we have tested four kinds of defects:

- a hole (15 mm diameter),
- a massive inclusion (8-mm-diameter, 3-mm-thick neodymium cylinder),
- a surface crack (30 × 1 mm and 2 mm depth),
- a through-crack (30 × 1 mm and 3 mm depth).

Here again the correlations are calculated in both undamaged and damaged plates and the subtraction between the two is performed. The noise is generated by friction. The beamformed images obtained with a massive inclusion and hole in the plate are displayed in Fig. 8. We observe that despite the fact that the inclusion is smaller than the hole, the spurious lobe level is higher for the hole. This can be explained by the fact that the scattering strength of a hole is quite small for flexural waves.

The next challenge is to detect a surface crack and a through-crack. Results for both introduced cracks are presented in Fig. 9. As can be seen, the defects are successfully detected in both cases because the cracks strongly interact with the acoustic field. The quality of the image obtained with the through-crack informs us about the satisfying reconstruction of the Green's functions. However, what is detected here is the strongest point of the defect, which is likely the edge of the groove, and the shape of the defect is not recovered. To achieve this, a complex inverse problem would have to be solved, which is completely beyond the scope of this paper.

The passive localization method presented here has been shown to be efficient and robust, at least provided

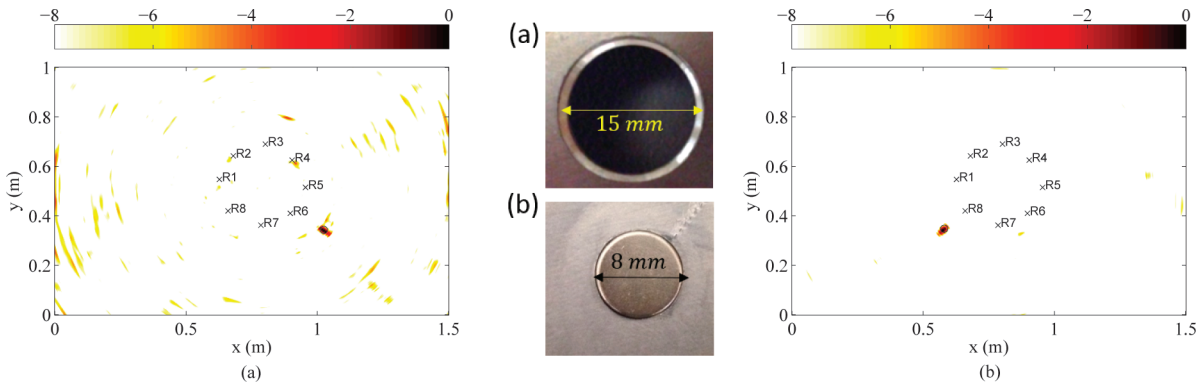

Fig. 8. Beamformed images obtained from $\Delta\mathbf{C}$ resulting from frictional noise, in decibels, for the corresponding defects shown in the center inset: (a) a 15-mm-diameter hole, centered at (1.025,0.343) m, and (b) a massive 8-mm-diameter inclusion, centered at (0.58,0.348) m.

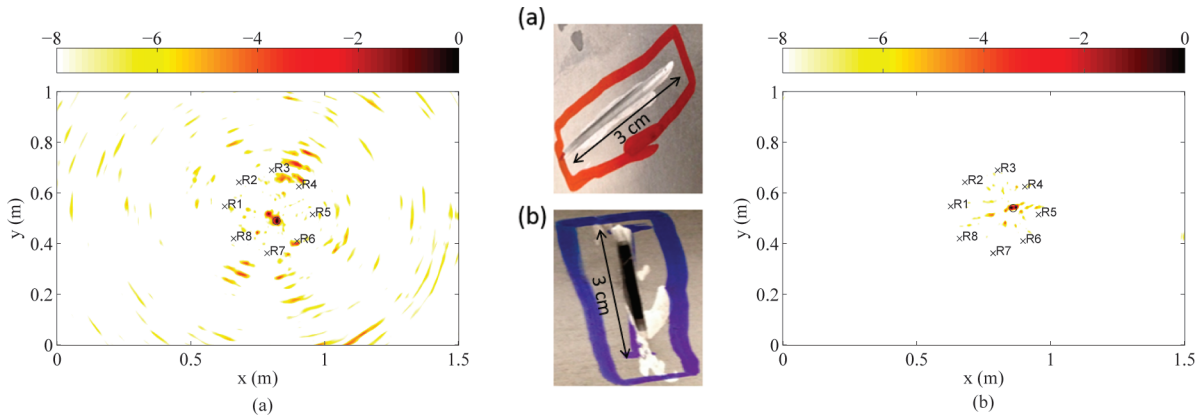

Fig. 9. Beamformed images obtained from $\Delta\mathbf{C}$ resulting from frictional noise, in decibels, for the corresponding defects shown in the center inset: (a) a surface crack, 30 × 1 mm and 2 mm depth, centered at (0.82,0.49) m, and (b) a through-crack, 30 × 1 mm and 3 mm depth, centered at (0.86,0.54) m.

some conditions are satisfied. This will be the subject of the discussion presented in the next section.

V. Robustness of the Method

Among the factors that can strongly influence the sensitivity of the method, there are the distribution and spatial stationarity of the noise sources and the number of receivers used to image the defect.

A. Spatial Distribution

In this section, we study the influence of the size of the area on which the noise is produced. Indeed, we have seen in Section II that an almost perfect reconstruction is obtained when the noise sources are homogeneously distributed over the whole plate.

In this part, contrary to the image obtained in Fig. 7, the noise is generated by friction over a small region of roughly 37 × 33 cm^2 size. For a given defect position, two different areas have been tested. The corresponding images are displayed in Fig. 10. The friction areas are indicated by a red rectangle on the images.

From these results, two conclusions can be drawn. First, the defect is still successfully localized. The smallness of the source area only increases the level of the spurious lobes. In other words, even if the Green's function reconstruction is not perfect, the beamforming of the spurious terms is sufficiently low and incoherent to remain below the level of the main lobe. Second, the position of the noise regions has a little influence on the defect localization. This last result lies in the fact that we take advantage of the reverberations over the plate. The properties of the quasi-diffuse field obtained in this condition only weakly depend on position.

Up to now, the correlation matrices with and without defect have been recorded when the noise is produced from the same area. In the next section, we will discuss the effect of removing this assumption.

B. Nonstationary Spatial Noise

When the noise is spatially nonstationary, the noise generation areas can be different between the reference and the damaged states. The experimental results obtained with frictional noise are shown on Fig. 11. The friction areas used in the defect-free acquisition are indi-

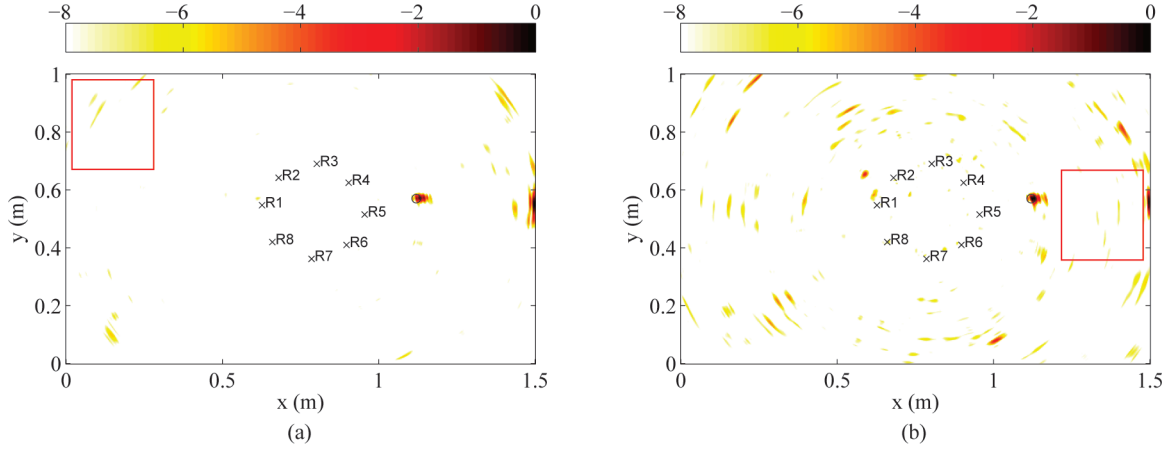

Fig. 10. Beamformed images (decibel scale) from $\Delta\mathbf{C}$ for two different noise areas. The noise is generated by friction inside the red rectangle.

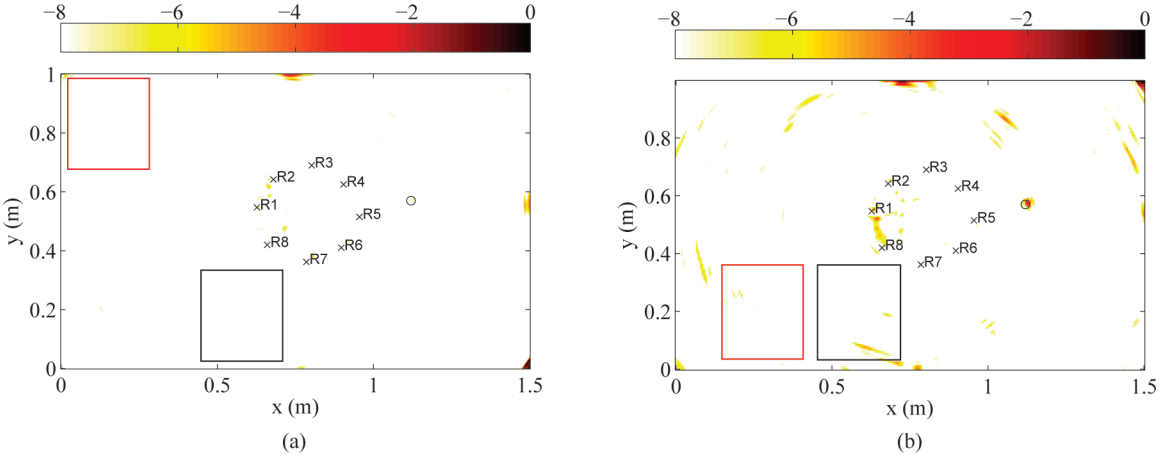

Fig. 11. Beamformed images obtained from frictional noise correlation, in decibels, showing the effect of spatially nonstationary noise for noise generation areas that are (a) widely separated and (b) close together. The red and black rectangles indicate the positions of the frictional regions in the undamaged and damaged states, respectively.

cated by a red rectangle on the images. The areas used in the acquisition with the defect are indicated by a black rectangle.

In the first case, the defect is no longer localized [Fig. 11(a)]. However, when the noise generation areas are sufficiently close to each other, the lobe on the defect appears again [Fig. 11(b)].

These results can be interpreted in the following way. First, for convenience, rewriting (2) under matrix formalism yields $\mathbf{C}(t) = [\mathbf{G}(t) - \mathbf{G}(-t)] \otimes f(t) + \mathbf{n}(t)$. Let us call A (respectively, B) the noise generation area used for the acquisition of the correlation matrix without (respectively, with) the defect. The expression of the differential matrix can then be written as

$$\Delta\mathbf{C} = [\Delta\mathbf{G}(t) - \Delta\mathbf{G}(-t)] \otimes f(t) + \mathbf{n}_{\mathrm{B}}(t) - \mathbf{n}_{\mathrm{A}}(t) + \delta\mathbf{n}_{\mathrm{B}}(t). \tag{7}$$

where $\Delta\mathbf{G}$ is the part of the Green's function due to the defect. The terms $\mathbf{n}_{\mathrm{A}}$ and $\mathbf{n}_{\mathrm{B}}$ are the spurious contributions, without the defect, obtained for generation area A and B, respectively. Finally $\delta\mathbf{n}_{\mathrm{B}}$ is the difference between the spurious terms obtained with and without defect when the noise is generated in area A. When the generation areas are identical (A = B), even if $\mathbf{n}_{\mathrm{A}}(t)$ is quite strong because area A is small compared with the total plate area, the difference between the correlation matrix cancels this contribution and only the small perturbation $\delta\mathbf{n}_{\mathrm{B}}(t)$ remains. The perturbation $\delta\mathbf{n}_{\mathrm{B}}(t)$ only slightly increases the spurious lobes on the images compared with the main lobe on the defect due to $\Delta\mathbf{G}(t) - \Delta\mathbf{G}(-t)$. However, for the case with different areas, $\mathbf{n}_{\mathrm{B}}(t) - \mathbf{n}_{\mathrm{A}}(t)$ might be the strongest contribution, possibly making the defect unlocalizable, as was observed in Fig. 11(a).

C. Number of Receivers

For practical application, it is interesting to evaluate the efficiency of the method with only a few receivers. The noise is generated by an acoustic source that is moved all over the plate surface. As shown on Fig. 7, when 8 receivers are used, the beamforming process is almost perfect. Now we perform this experiment with the correlation matrix computed from 6 and 4 receivers.

As can be seen on Fig. 12, the defect is still localized even with only 4 receivers. This is because the process is performed over a wide frequency range. However, the level of spurious lobes obviously grows as the number of receivers decreases. This is quantified in Table I (where 0 dB corresponds to the maximum of the defect lobe). This phenomenon is caused by two joint effects. First, the cancellation of the unwanted contribution $\mathbf{n}(t)$ is less efficient when fewer sensor pairs are involved. Second, the beamforming performance is degraded when the array aperture and sampling are decreased. Actually, as soon as the Green's functions are correctly estimated by cross-correlation, the detection ability is dictated by the classical law of beamforming array processing (resolution related to the array aperture).

These encouraging results offer promising avenues to imaging defects with a small number of receivers. To our knowledge, there are no works cited that obtained similar results with such a low number of receivers.

VI. Conclusion

In this work, we have presented an experimental validation of a passive technique for defect localization in metallic plates. We have successfully detected defects from noise

TABLE I. Spurious Lobe Levels Excluding the Location of the Focal Spot (A Half-Wavelength Around 0 dB).

	Number of receivers				
	8	6	5	4	3
Spurious lobes level (dB)	−7.20	−5.28	−3.82	−2.99	−1.10

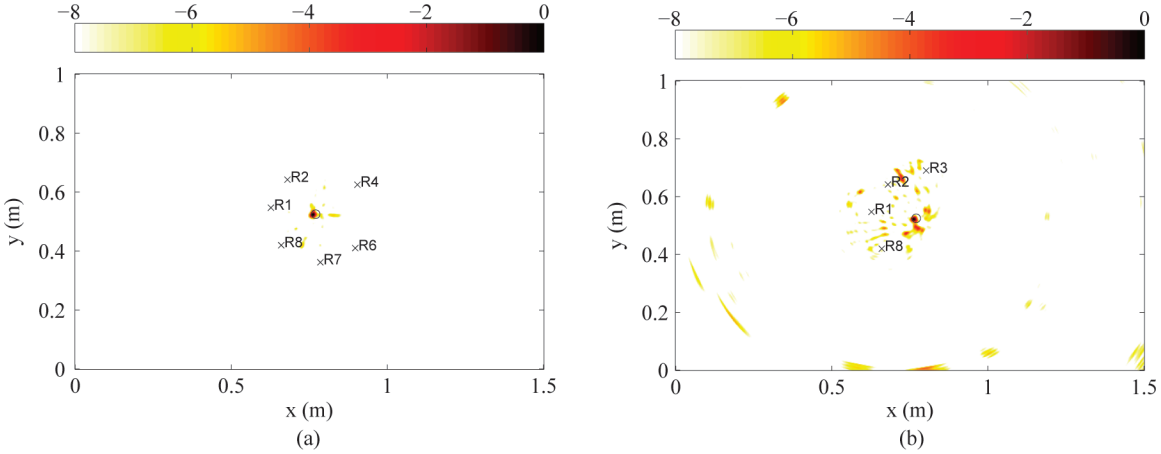

Fig. 12. Beamformed images obtained from acoustic noise correlation, in decibels: (a) 6 receivers and (b) 4 receivers.

generated by different sources between 10 and 40 kHz. Using a laser vibrometer experiment, we have shown that the fidelity of the estimation of the transient responses depends on the spatial distribution of noise. Nevertheless, because of the differential acquisition of the correlation technique, we have shown that the defect localization capability is more sensitive to spatial nonstationarity of the noise than to the quality of the Green's function estimation. Hence, we have experimentally shown that the method is suitable and robust to detect holes, massive inclusions, and even surface or through cracks in the plate.

These preliminary experiments are very promising for structural health monitoring applications and are expected to be of considerable value in the future. Further work will focus on a full theoretical development to be able to predict the spurious lobe levels as a function of the involved parameters. We are also currently working on this technique to provide some basic characteristic parameters of the defect.

References

[1] R. L. Weaver and O. I. Lobkis, "Ultrasonics without a source: Thermal fluctuation correlations at MHz frequencies," *Phys. Rev. Lett.*, vol. 87, no. 13, art. no. 134301, 2001.

[2] S. M. Rytov, "On thermal agitation in distributed systems," *Sov. Phys. Dokl.*, vol. 1, pp. 555–559, May 1956.

[3] M. L. Levin and S. M. Rytov, "'Kirchhoff' form of fluctuation-dissipation theorem for distributed systems," *Sov. Phys. JETP*, vol. 38, no. 4, pp. 688–692, 1974.

[4] R. Snieder, "Extracting the Green's function from the correlation of coda waves: A derivation based on stationary phase," *Phys. Rev. E*, vol. 69, no. 4, art. no. 046610, 2004.

[5] C. E. Weller, "Seismic exploration method," U.S. Patent US3812457A, May 21, 1974.

[6] J. F. Claerbout, "Synthesis of a layered medium from its acoustic transmission response," *Geophysics*, vol. 33, no. 2, pp. 264–269, 1968.

[7] T. L. Duvall, S. M. Jefferies, J. W. Harvey, and M. A. Pomerantz, "Time-distance helioseismology," *Nature*, vol. 362, no. 6419, pp. 430–432, 1993.

[8] B. Artman, "A return to passive seismic imaging," Stanford Exploration Project, Stanford, CA, 2002, vol. 111, pp. 361–369.

[9] N. M. Shapiro and M. Campillo, "Emergence of broadband Rayleigh waves from correlations of the ambient seismic noise," *Geophys. Res. Lett.*, vol. 31, no. 7, art. no. L07614, 2004.

[10] R. Weaver and O. Lobkis, "On the emergence of the Green's function in the correlations of a diffuse field: Pulse-echo using thermal phonons," *Ultrasonics*, vol. 40, pp. 435–439, May 2002.

[11] V. I. Mirgorodskii, V. V. Gerasimov, and S. V. Peshin, "Experimental studies of passive correlation tomography of incoherent acoustic sources in the megahertz frequency band," *Acoust. Phys.*, vol. 52, no. 2, pp. 606–612, 2006.

[12] P. Roux and W. A. Kuperman, and the NPAL Group, "Extracting coherent wave fronts from acoustic ambient noise in the ocean," *J. Acoust. Soc. Am.*, vol. 116, no. 4, pp. 1995–2003, 2004.

[13] K. G. Sabra, P. Roux, M. Thode, G. L. D'Spain, W. S. Hodgkiss, and W. A. Kuperman, "Using ocean ambient noise for array self-localization and self-synchronization," *IEEE J. Ocean. Eng.*, vol. 30, no. 2, pp. 338–347, 2005.

[14] K. G. Sabra, S. Conti, P. Roux, and W. A. Kuperman, "Passive in vivo elastography from skeletal muscle noise," *Appl. Phys. Lett.*, vol. 90, no. 19, art. no. 194101, 2007.

[15] C. R. Farrar and G. H. James, "System identification from ambient vibration measurements on a bridge," *J. Sound Vibrat.*, vol. 205, no. 1, pp. 1–18, 1997.

[16] K. G. Sabra, A. Srivastava, F. L. di Scalea, I. Bartoli, P. Rizzo, and S. Conti, "Structural health monitoring by extraction of coherent guided waves from diffuse fields," *J. Acous. Soc. Am.*, vol. 123, no. 1, pp. EL8–EL13, 2008.

[17] E. Larose, P. Roux, and M. Campillo, "Reconstruction of Rayleigh-Lamb dispersion spectrum based on noise obtained from an air-jet forcing," *J. Acoust. Soc. Am.*, vol. 122, no. 6, pp. 3437–3444, 2007.

[18] E. Moulin, N. Abou Leyla, J. Assaad, and S. Grondel, "Applicability of acoustic noise correlation for structural health monitoring in nondiffuse field conditions," *Appl. Phys. Lett.*, vol. 95, no. 9, art. no. 094104, 2009.

[19] L. Chehami, E. Moulin, J. de Rosny, C. Prada, O. Bou Matar, F. Benmeddour, and J. Assaad, "Detection and localization of a defect in a reverberant plate using acoustic field correlation," *J. Appl. Phys.*, vol. 115, no. 10, art. no. 104901, 2014.

[20] H. Lamb, "On the propagation of tremors over the surface of an elastic solid," *Philos. Trans. R. Soc. Lond.*, vol. 203, pp. 1–42, Jan. 1904.